A Circular Life-cycle Paradigm for Bio-derived Dual-ligand Cu-MOFs: from Scalable Manufacturing to Greenhouse Gas Mitigation

*Zhang-Ye Han[1], Xuefeng Bai[1], Rui Li[*1], Qiang Chen, and Jian-Rong Li[*1]*

1. Beijing Key Laboratory for Green Catalysis and Separation and Department of Chemical Engineering, College of Materials Science and Engineering, Beijing University of Technology, Beijing, P. R. China 100124.

* Corresponding authors.

E-mail addresses: jrli@bjut.edu.cn (J.-R. Li), lirui1@bjut.edu.cn (R. Li).

1. Materials and methods

1.1 Materials and reagents

Copper (II) chloride dihydrate ($CuCl_2 \cdot 2H_2O$) was purchased from Sinopharm Chemical Reagent Co., Ltd. 2,2-oxydiacetic acid (ODA) was purchased from Bide Pharmatech Co., Ltd. N, N-Dimethylformamide (DMF), ethanol (EtOH) and methanol (MeOH) were purchased from Tianjin Fuyu Fine Chemical Co., Ltd. Sodium hydroxide (NaOH) was purchased from Anhui Zesheng Technology Co., Ltd. Anhydrous cupric sulfate ($CuSO_4$), adenine (AD), succinic acid (SA), glutaric acid (GA), and acetic acid (HOAc) were purchased from HEOWNS Biochem LLC. Hydroxyethyl cellulose (HEC) and polyvinyl alcohol (PVA) were purchased from Shanghai Aladdin Biochemical Technology Co., Ltd. Deionized (DI) water used in all experiments was purified with a Siemens Ultra Clear TWF water purification system. CO_2 (> 99.999 %), CH_4 (> 99.999 %), SF_6 (> 99.999 %), He (> 99.999 %), N_2 (> 99.999 %) and gas mixtures of SF_6/ N_2 (1/9, v/v), CO_2/N_2 (15/85, v/v), and CO_2/ CH_4 (1/1, v/v) were purchased from Beijing Beiyang United Gas Co., Ltd. All chemicals were used as received without any further purification.

1.2 Characterization

1.2.1 Powder X-ray diffraction (PXRD)

PXRD was conducted to verify the structure and phase purity of bio-based Cu-MOFs. The data was collected with a Rigaku SmartLab3 diffractometer (Cu Kα radiation, λ = 1.542 Å) from 5° to 30° (2θ range) at a scan rate of 5 ~ 10° per minute. The sample powders were spread on glass substrates for the tests. The simulated XRD pattern was generated from the crystal structure (i.e., the cif file).

1.2.2 BET surface area and pore size distribution analysis

Nitrogen adsorption–desorption isotherms were measured at 77 K to determine the specific surface area and pore structure of the samples. Prior to the measurements, all samples were degassed under vacuum at 120 °C for over 12 h to remove adsorbed impurities and moisture.

1.2.3 Scanning electron microscope (SEM)

The SEM images were collected by a HITACHI SU3500 scanning electron microscope operating at 15～20 kV. Prior to imaging, samples were ultrasonically dispersed in ethanol to form a uniform dilute suspension. A few microliters of the suspension were drop-casted onto silicon slices and allowed to dry under ambient conditions.

1.2.4 Adsorption experiments

The Micromeritics ASAP 2020 volumetric adsorption apparatus and Microtrac Belsorp Max II gas adsorption analyzer were used to measure the adsorption isotherms of SF_6, CO_2, CH_4 and N_2 at 273 and 298 K. The temperature was precisely controlled by a recirculating control system containing a mixture of ethylene glycol and water (298 K) or an ice-water mixture (273 K). The as-synthesized MOF samples were pretreated at 393 K for 12 h under vacuum conditions to remove the guest molecules before the measurements.

1.2.5 Breakthrough experiments

To verify the ability of BUT-321 to separate the gas mixtures (SF_6/N_2, CO_2/N_2, and CO_2/CH_4) under dynamic conditions, breakthrough experiments were performed at 298 K and 1 bar. The sample powder (about 1.792 g for SF_6/N_2, 1.3638 g for CO_2/N_2, and 1.859 g for CO_2/CH_4) was filled into a cylindrical stainless steel breakthrough column (4.5 × 210 mm) and was degassed at 393 K under vacuum for 12 h. The flow rate and

the pressure at the inlet are controlled by a mass flow controller and a pressure sensor, respectively. The mixed gases were fed into the breakthrough column at a flow rate of 5.0 mL/min. The effluent gas was examined by a gas chromatograph.

1.3 Calculations details

1.3.1 Brunaue-Emmett-Teller (BET) surface areas

The BET surface areas of samples were evaluated from the N_2 adsorption isotherms at 77 K using *Eq 1* below.

$$S_{BET} = \frac{N_A \partial}{22414\,(K + I)} \qquad (Eq\ 1)$$

where N_A is Avogadro's constant; ∂ is the cross-sectional area of each adsorbate molecule; and 22414 is the volume (mL) of 1 mole ideal gas at the standard temperature and pressure. K and I represent the slope and intercept of the fitted line, respectively.

1.3.2 Calculation of isosteric heat of adsorption

The bonding energy between the adsorbate molecules and the adsorbent lattice atoms are reflected in the isosteric heat of adsorption (Q_{st})[1], which is defined as:

$$Q_{\mathrm{st}} = R\sum_{i=0}^{m} a_i N^i \qquad (Eq\ 2)$$

$$\ln P = \ln N + \frac{1}{T}\sum_{i=0}^{m} a_i N^i + \sum_{j=0}^{m} b_j N^j \qquad (Eq\ 3)$$

where Q_{st} is the coverage-dependent enthalpy of adsorption; R is the universal gas constant; P represents the pressure (mmHg); T represents the temperature (K); N is the adsorbed amount (mg/g); a_i and b_j are Virial coefficients and m, n represent the numbers of coefficients used to adequately describe the adsorption curves. The values of a_0 through a_m were used to calculate the isosteric heat of adsorption using *Eq 2*.

1.3.3 Calculation of E-factor

E-factor[2] is an important indicator in green chemistry, defined as the ratio of the total mass of waste generated during the chemical process to the mass of the target product. As a key indicator for evaluating the environmental impact of synthetic routes, a lower

E-factor value indicates a cleaner and more efficient process. In this study, E-factor was used to quantitatively assess the greenness of the new green synthesis process of BUT-321 compared to the traditional synthesis method.

$$\text{E - factor} = \frac{Mass\ of\ total\ waste}{Mass\ of\ product} \quad (Eq\ 4)$$

In the formula, *Mass of total waste* represents the total mass of the waste generated during the synthesis of BUT-321, including the solid waste and solvents; *Mass of product* is the quality of the obtained BUT-321 product.

1.3.4 Reaction mass efficiency (RME)

The calculation formula for Reaction Mass Efficiency[2], another critically important indicator in green chemistry, is as follows:

$$RME\ (\%) = m(Product)/\sum m(Raw\ materials) * 100\% \quad (Eq\ 5)$$

In the formula, *m(Product)* represents the mass of BUT-321; $\sum m(Raw\ materials)$ is the quality of the total mass of all reactants.

1.3.5 Fitting of gas adsorption isotherms

The experimentally measured CH_4 and N_2 uptakes of samples at 298 K were fitted with the 1-site, 2-site, or 3-site-Langmuir isotherm models:

1-site-Langmuir isotherm model:
$$N = A \times \frac{bP^C}{1 + bP^C} \quad (Eq\ 6)$$

2-site-Langmuir isotherm model:
$$N = A \times \frac{b_1P^{C_1}}{1 + b_1P^{C_1}} + A_2 \times \frac{b_2P^{C_2}}{1 + b_2P^{C_2}} \quad (Eq\ 7)$$

3-site-Langmuir isotherm model:
$$N = A \times \frac{b_1P^{C_1}}{1 + b_1P^{C_1}} + A_2 \times \frac{b_2P^{C_2}}{1 + b_2P^{C_2}} + A_3 \times \frac{b_3P^{C_3}}{1 + b_3P^{C_3}} \quad (Eq\ 8)$$

where *N* is the adsorbed amount per gram of adsorbent (mmol/g); *P* is the pressure of the bulk gas at equilibrium with the adsorbed phase (kPa); A is the saturation capacities of sites A (mmol/g); b is the affinity coefficients of sites A (1/kPa); and C represents the deviations from an ideal homogeneous surface. The fitting parameters of *Eqs 4-6* are listed in the lower right tables of corresponding Figures.

1.3.6 Ideal adsorbed solution theory (IAST)

IAST calculations were performed to evaluate the SF_6/N_2, CO_2/N_2, and CO_2/CH_4 separation performance. The adsorption selectivity of component 1 over component 2 in a binary mixture can be defined by:

$$S_{1,2} = \frac{q_1/q_2}{y_1/y_2} \qquad (Eq\ 9)$$

In *Eq 7*, the q_1 and q_2 represent the equilibrated molar uptakes of each component (mol/kg); y_1, and $y_2 = 1 - y_1$, represent the mole fractions of components 1 and 2 in the bulk inlet gas, respectively. IAST calculations were performed at 298 K in the pressure range from near zero to 101 kPa.

1.3.7 Calculation of the dynamic adsorption capacity

The dynamic uptake of target gas is calculated as:

$$Q = \frac{v \times V\%}{22.4}\int_{t0}^{t1}(C_0 - C_i)\,dt = \frac{v \times V\%}{22.4}S \qquad (Eq\ 10)$$

where *v* refers to the flow rate of the gas mixture, *V%* refers to the molar fraction of target gas. S is the highlighted area shown in the breakthrough curves (Figure S11).

1.3.8 Computational Details.

DFT calculations were carried out using the CP2K code[3]. BUT-321 showed no significant adsorption-induced structural deformation or gate-opening behavior, so its macroscopic flexibility was not explicitly considered in DFT calculations. However, ligand hydrogen atoms were relaxed during geometry optimization to capture local host-guest interactions. All reported adsorption energies correspond to optimized configurations at the zero-coverage limit, without lateral guest-guest interactions. All calculations employed mixed Gaussian and planewave basis sets. Core electrons were represented with norm-conserving Goedecker-Teter-Hutter pseudopotentials[4-6], and the valence electron wavefunction was expanded in a double-zeta basis set with polarization functions[7] along with an auxiliary plane wave basis set with an energy cutoff of 360 Ry. The generalized gradient approximation exchange-correlation function of Perdew, Burke, and Enzerhof (PBE)[8] was used. Each configuration was optimized with the OT algorithm with SCF convergence criteria of 1.0×10^{-8} au. To

compensate for the long-range van der Waals dispersion interaction between the adsorbate and the MOFs, the DFT-D3 scheme[9] with an empirical damped potential term was added into the energies obtained from exchange-correlation functional in all calculations.

The adsorption energy between the adsorbate and the BUT-321 can be calculated using the following equation:

$$\Delta E_{ads} = E_{adsorbate@MOF} - E_{MOF} - E_{adsorbate} \quad (Eq\ 11)$$

In Eq. (11), $E_{adsorbate@MOF}$ and E_{MOF} represent the total energies of the substrate with and without adsorbate, respectively. $E_{adsorbate}$ is the energy of the adsorbate. According to this equation, a negative adsorption energy suggests a stable adsorption configuration.

2. Experimental Section

2.1 Traditional solvothermal synthesis of BUT-321[10]

$CuCl_2 \cdot 2H_2O$ (0.06 mmol, 10 mg), 2,2-oxydiacetic acid (0.04 mmol, 5 mg), and adenine (0.04 mmol, 5 mg) were added to a ternary mixed solvent of N, N-dimethylformamide (DMF, 2 mL), methanol (MeOH, 1 mL), and deionized water (H_2O, 1 mL) and stirred for 10 min at room temperature. Then, the mixture was heated at 353 K for 48 h. The green crystal of BUT-321 was obtained after washing with DMF to remove unreacted species.

Scale-up of traditional solvothermal synthesis. Large-scale BUT-321 powder could be obtained by heating and stirring $CuCl_2 \cdot 2H_2O$ and the two ligands (stoichiometric ratio = 2:1:1) in a mixture of DMF (0.25 L), MeOH (0.5 L), and water (0.2 L) at 353 K for 24 h under ambient pressure.

2.2 Green synthesis of bio-based dual-ligand Cu-MOFs

Synthesis of $Cu_2(AD)_2ODA$ (BUT-321): NaOH, 2,2-oxydiacetic acid (ODA), and adenine (AD) were added to a binary mixed solvent of H_2O (3 mL) and ethanol (EtOH, 4mL) according to a molar ratio of 3.4: 1: 1.7. Then, the mixture was ultrasonicated until forming a clear solution. With the addition of 3 mL 0.67 M $CuSO_4$(aq), the mixture

was heated at 353 K for 24 h. The green BUT-321 crystals were obtained after washing with deionized water.

Synthesis of $Cu_2(AD)_2SA$: The synthesis protocol follows that of BUT-321 except succinic acid (SA) was used instead of ODA.

Synthesis of $Cu_2(AD)_2GA$: The synthesis protocol follows that of BUT-321 except glutaric acid (GA) was used instead of ODA.

Synthesis of $Cu_2(AD)_2OAc_2$: The synthesis protocol follows that of BUT-321 except acetic acid (HOAc) was used instead of ODA.

2.3 Optimization of NaOH usage

The same green synthesis protocol of BUT-321 (as shown in section 2.2) was employed, with the NaOH usage changed to varied amounts of 0, 0.1, 0.165, 0.18, and 0.19 g.

2.4 Optimization of the H_2O/EtOH ratio

The synthesis protocol follows the one of BUT-321 (as shown in section 2.2) except varying H_2O: EtOH ratios of 6/4, 7/3, 8/2, 9/1, and 10/0 (v/v) were employed.

2.5 Large-scale green synthesis of BUT-321

NaOH, ODA, and AD (molar ratio 3.4: 1: 1.6) were added to a mixed solvent of H_2O (4 L) and EtOH (1.6 L) in a 10 L jacketed glass reactor. After stirred for 10 min, 2.4 L 0.67 M $CuSO_4$(aq) was introduced. The mixture was then heated at 353 K for 24 h. After cooling to room temperature, 0.412 kg green BUT-321 product (≈ 98% yield, based on the Cu^{2+}) was obtained after washing with deionized water.

2.6 Green preparation of MOFs pellets (small scale)

Preparation of BUT-321/PVA pellets. An appropriate amount of water and 0.03 g PVA was added to 0.97 g BUT-321-S powder in small amounts many times. The resulting mixture was shaped into 2-4 mm pellets by extrusion molding. The pellets were heated at 100 °C for 24 h, resulting in a BUT-321 content of 97%

Preparation of BUT-321/HEC pellets. The same preparation protocol for BUT-321/PVA pellets was adopted, except that 0.03 g HEC was used instead of PVA.

2.7 Green preparation of MOFs pellets (large scale)

An appropriate amount of water and 3 g HEC was added to 97 g BUT-321-S powder by small amounts for many times. The resulting mixture was shaped into 2-3 mm sized pellets by granulator. The large-scale BUT-321/HEC pellets with 97% loading were heated at 100 °C for 24 h.

2.8 Green regeneration

0.3 g mechanically degraded MOF powder was immersed in 5 mL post-synthesis supernatant. The suspension was acidified with 2 mmol H_2SO_4 and ultrasonicated to homogeneity. Similarly, 5 mL post-synthesis supernatant was mixed with 4 mmol NaOH and the resultant solution was decanted into the acidified regeneration suspension containing the discarded MOF. The resulting mixture was placed in an oven and reacted at 80 °C for 24 h. The final product was washed and recovered by filtration, affording 0.25 g reconstructed MOF (85% yield).

Tables

Table S1. Comparison of green chemistry metrics between the developed green synthesis protocol and the conventional solvothermal approach.

Green chemistry metrics	Traditional Synthesis[10]	This work	Advancement in sustainability
E-factor	27.4 (water included) 21.2 (water excluded)	19.4 (water included) 3.8 (water excluded)	29.2% reduction 82.1% reduction
Reaction mass efficiency	36.7%	56.3%	53.4% increase
Solvent	DMF/ MeOH/ H_2O	H_2O/ EtOH	Safer solvent
Process residuals (solvent excluded)	Excess ligand (AD), metal salt, and acid	Primarily Na_2SO_4	Minimized waste

Table S2. SF_6 adsorption performances of representative porous adsorbents at 298 K, collected from previous literature. The performance of BUT-321 was shown as a comparison.

Adsorbent	S_{BET} (m^2/g)	SF_6 uptake (mmol/g)	Q_{st} (kJ/mol)	Ref
BUT-321	**843**	**3.05**	**31.4**	**This work**
GNU-3a	930	2.75	22.9	11
UiO-66	1074	1.6	33	12
CAU-17	496	1.45	~35	13
CAU-33	373	1.56	—	13
SU-101	344	0.8	~30	13
MOF-74(Mg)	1631	6.42	32.0	14
$Ni(ina)_2$	470	2.84	3.4	15
Yb-TBAPy	940	2.33	33	16
Tm-TBAPy	815	1.83	32	16
Hf-TBAPy	760	1.38	30	16
HKUST-1a	1090	3.56	24.9	17
HKUST-1b	1135	4.06	15.2	17
HKUST-1c	1328	4.98	9.5	17
CAU-10-py	684.4	1.76	32.6	18
UiO-66-Br_2	616	0.92	44.5	12
$Ni(pda)_2$	807	3.5	24	15
SBMOF-1	150	1.03	32.5	19
$Co(HCOO)_6$	330.1	2.18	—	20
HBU-21	381	0.94	25	21
BUT-53	874	3.55	23.8	22
$Ni(3\text{-mpba})_2$	835	2.83	30.2	23
$Co(3\text{-mpba})_2$	629	3.25	26.8	23
$Ni(ina)(bdc)_{0.5}$	610	1.81	25.8	24
$Ni(3\text{-min})(bdc)_{0.5}$	628	2.25	31.3	24

Table S2. Continue

Adsorbent	S_{BET} (m^2/g)	SF_6 uptake (mmol/g)	Q_{st} (kJ/mol)	Ref
Cu-MOF-NH_2	2145	7.88	55.2	25
Ni(adc)$(dabco)_{0.5}$	743	2.38	47.6	26
Zn(TMBDC)$(DABCO)_{0.5}$	975	4.61	45.2	27
Ni(NDC)(TED)0.5	1306	4.5	47.6	28
V-TCPB	1370	3.07	30.48	29
Ga-TCPB	1484	2.95	30.44	29
Co(BPZ)	946	3.25	3.19	30
Ni(BPZ)	756	2.5	49.9	30
Zn(BPZ)	955	3.0	31	30
MIL-100(Fe)	1619	1.66	20.5	31
Zeolite-13X	707	~2.2	23	31

Table S3. CO_2 adsorption performances of representative porous adsorbents at 298 K, gathered from the previous literature. The performance of BUT-321 was shown as a comparison.

Adsorbent	S_{BET} (m^2/g)	CO_2 uptake (mmol/g)	Q_{st} (kJ/mol)	Ref
BUT-321	**843**	**3.67**	**24.0**	**This work**
GNU-3a	930	1.36	19.8	11
UiO-66	838	2.27	—	32
CAU-17	496	2.35	~25	13
CAU-33	373	1.96	~20	13
SU-101	344	2.13	~20	13
MOF-74(Mg)	1495	~8.0	47	33
Ni$(3\text{-ain})_2$	359	3.72	31.8	34
Yb-TBAPy	940	2.7	25	16
Tm-TBAPy	815	2.09	22	16
Hf-TBAPy	760	1.44	22.25	16
HKUST-1	1760	5.33	25.9	35
CALF-20	528	4.07	39.0	36
MIL-120	590	3.87	40.0	37
MIP-202	235	0.56	30.7	38
SIFSIX-2-Cu-i	735	4.25	35.0	39
SIFSIX-3-Zn-i	250	2.3	45.0	39
SIFSIX-14-Cu-i	612	2.54	37.7	39
MOF-808-Gly	1971	2.03	46.0	40
UTSA-120a	638	5.0	27–31	41
ZU-66	177	4.56	35	42
Cu-AD-SA	846	3.47	22.4	43
$Al(HCOO)_3$	588	4.8	47.7	44
FJI-H38	296	2.33	27	45

Table S3. Continued

Adsorbent	S_{BET} (m^2/g)	CO_2 uptake (mmol/g)	Q_{st} (kJ/mol)	Ref
NJFU-5	473	1.65	29.9	46
MOF-11	606	4.63	45.6	47
MUF-4	1094	3.17	24.4	48
ZJU-620(Al)	1347	4.25	12	49
CoIPA	283	0.82	30.2	50
ZIF-8	1475	0.82	—	51
PCN-250(Fe_3)	1470	0.57	26.6	52
PCN-250(Fe_2Co)	1653	0.51	28.6	52
IISERP-MOF28	497	3.1	32	53
ZnF(daTZ)	890	3.3	33	54
CU-4	—	3.1	36.9	55
TYUT-ATZ	275	2.8	24.6	56
Zn-MOF(1a)	317	2.77	29.8	57
$ZnAtzCO_3$	455	2.8	32.6	58
SMOF-SIFSIX-1	363	1.5	40.98	59

Table S4. The dynamic adsorption capacities for greenhouse gases compared with the corresponding static adsorption capacities under identical conditions.

	0.1 ar SF_6 ($cm^3\ g^{-1}$)	0.15 bar CO_2 ($cm^3\ g^{-1}$)	0.5 bar CO_2 ($cm^3\ g^{-1}$)
Gas uptake	28.1	20.3	56.1
Dynamic adsorption	27.5	19.7	55.4

Table S5. Comparative evaluation of SF_6, CO_2, CH_4, and N_2 sorption capacities at 298 K between pristine BUT-321-S and scaled BUT-321/HEC (large scale) samples.

	SF_6 uptake ($cm^3\ g^{-1}$)	CO_2 uptake ($cm^3\ g^{-1}$)	CH_4 uptake ($cm^3\ g^{-1}$)	N_2 uptake ($cm^3\ g^{-1}$)
BUT-321-powder	68.3	82.1	14.6	4.37
BUT-321-shaped	61.0	76.1	13.4	4.22
Uptake loss (%)	7.9%	4.4%	5.4%	0.4%

Note: The uptake loss of gas is calculated from: $(Q_{Powder}-Q_{Shape}/0.97)/Q_{powder}$

Table S6. Comparative evaluation of SF_6, CO_2, CH_4, and N_2 sorption capacities at 273 K between pristine BUT-321-S and scaled BUT-321/HEC (large scale) samples.

	SF_6 uptake ($cm^3\ g^{-1}$)	CO_2 uptake ($cm^3\ g^{-1}$)	CH_4 uptake ($cm^3\ g^{-1}$)	N_2 uptake ($cm^3\ g^{-1}$)
BUT-321-powder	85.8	122.3	29.6	8.65
BUT-321-shaped	75.0	109.4	26.0	6.43
Uptake loss (%)	9.9%	7.8%	9.4%	23.4%

Note: The uptake loss of gas is calculated from: $(Q_{Powder}-Q_{Shape}/0.97)/Q_{powder}$

Figures

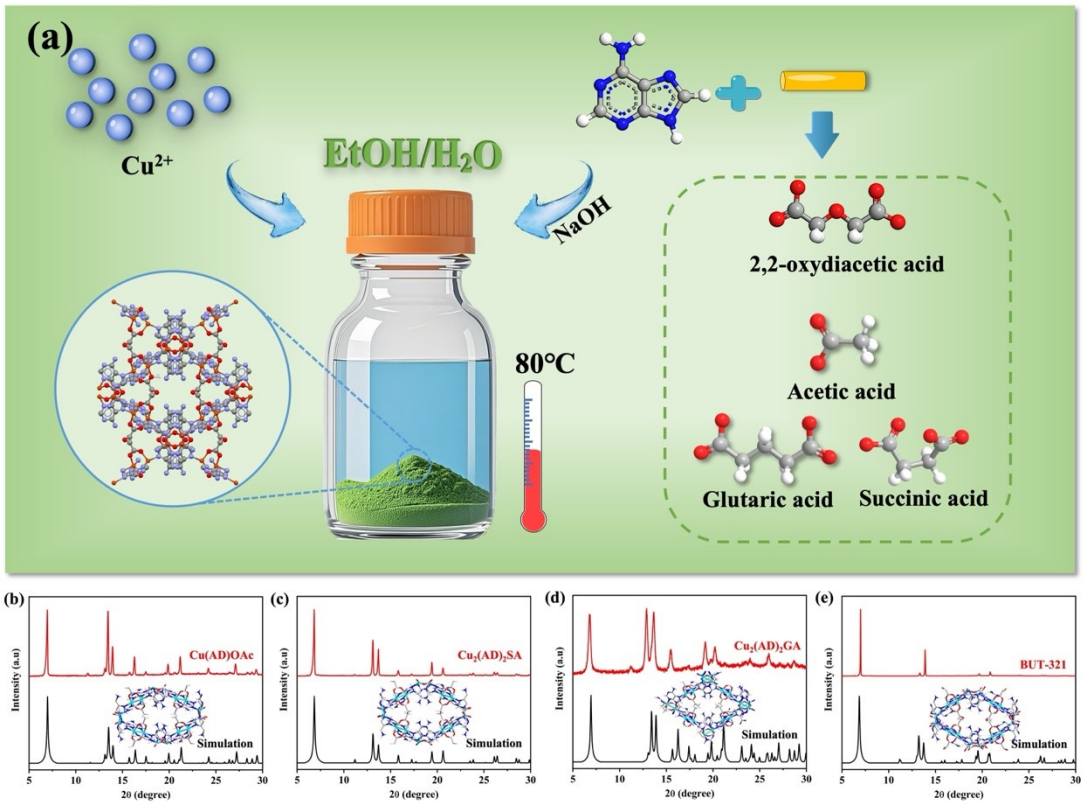

Figure S1. (a) Schematic illustration of the green and scalable synthesis strategy for biomass-derived Cu-MOFs under mild conditions. (b-e) PXRD patterns and crystal structures of (b) $Cu_2(AD)_2OAc$, (c) $Cu_2(AD)_2SA$, (d) $Cu_2(AD)_2GA$ and (e) BUT-321 synthesized via the base-assisted strategy in ethanol-mediated aqueous solution. The high PXRD diffraction signals indicate the superior crystallinity of the MOF samples, substantiating the universal applicability of this method.

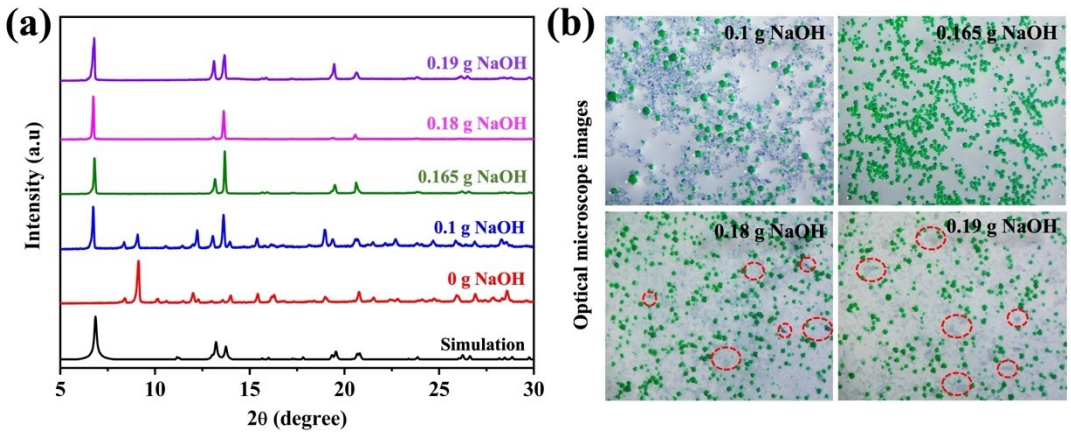

Figure S2. (a) PXRD patterns and (b) optical micrographs of BUT-321 synthesized with altered NaOH usages. The NaOH dosage is found to strongly impact the phase purity of BUT-321. Clear impurity is observed when the alkali amount is insufficient,

whereas a distinct impurity emerges (red circles in the micrographs) with excessive alkali.

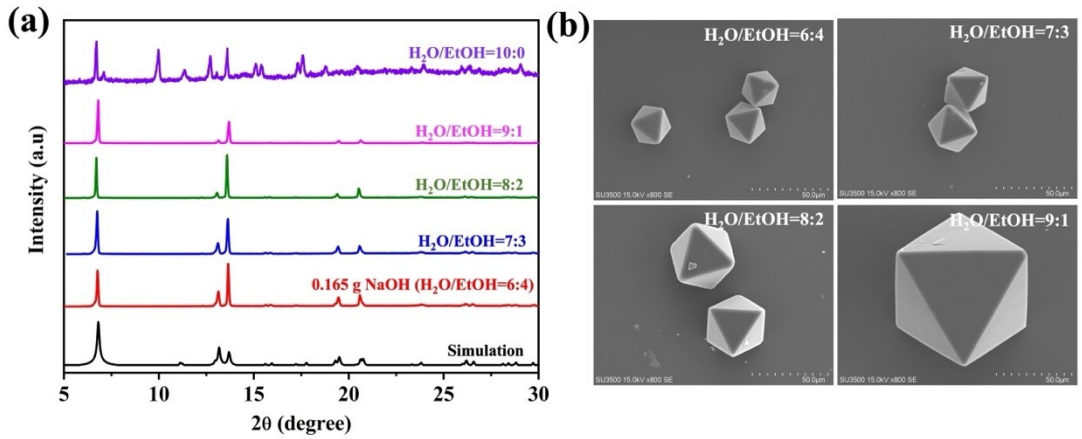

Figure S3. (a) PXRD patterns and (b) electron micrographs of BUT-321 obtained with altered H_2O/EtOH ratio. Reduced ethanol content led to larger crystals, whereas the absence of ethanol caused the formation of impurity.

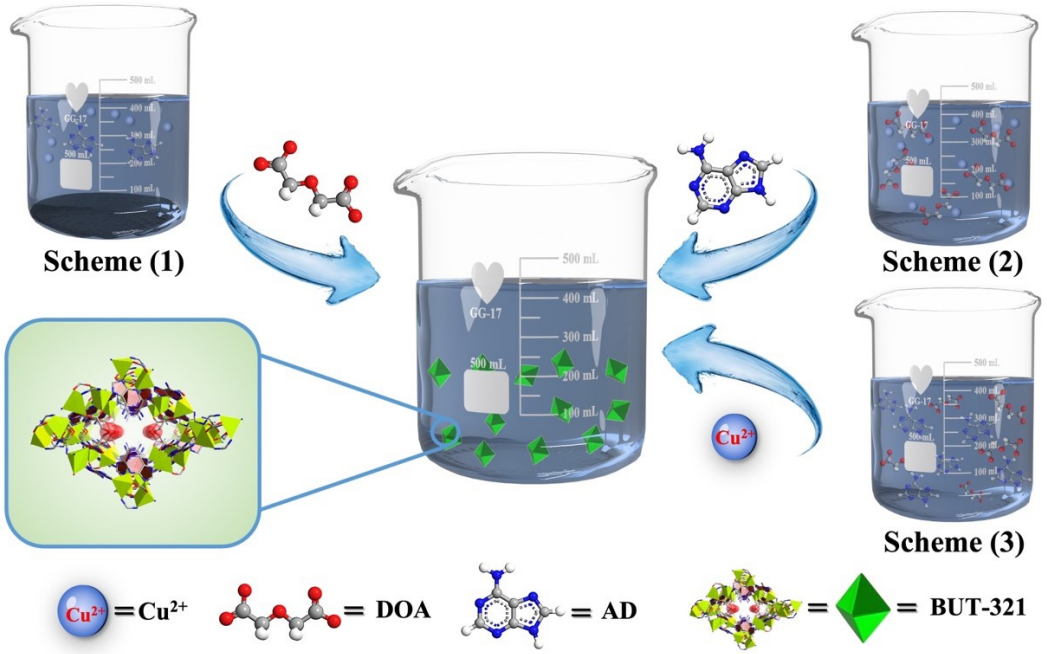

Figure S4. Schematic illustration of BUT-321 crystallization pathways with altered addition sequence of ingredients. The cartoon icons representing different ingredients and the MOF product are labelled under the scheme.

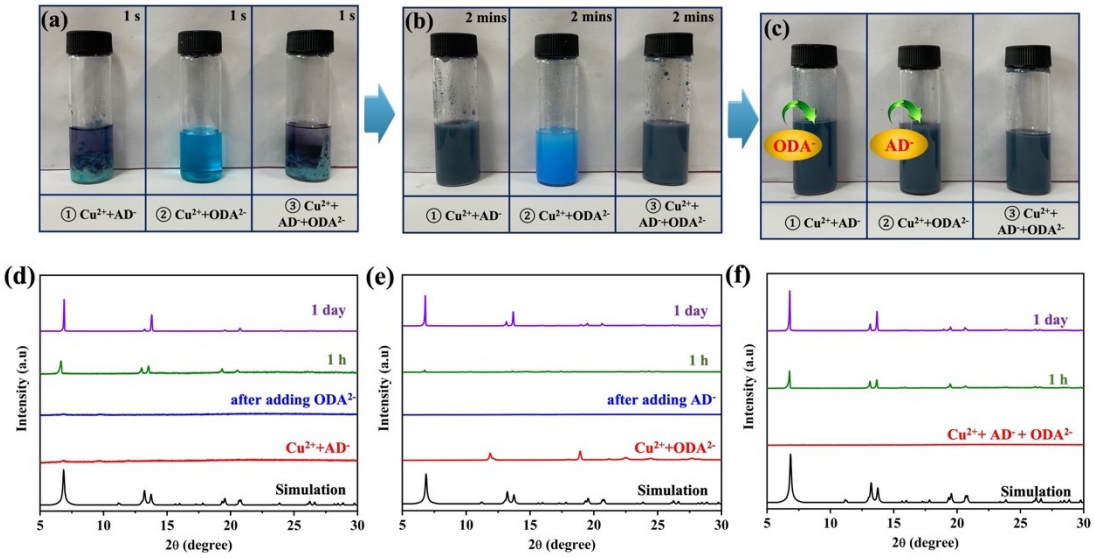

Figure S5. Effects of ingredient addition sequence on synthesis mixtures. Cu^{2+} was initially mixed with AD^{-} (scenario 1) or ODA^{2-} (scenario 2) and aged at room temperature for (a) 1 s and (b) 2 min. (c) Subsequently, the second ligand was added. The mixture whose two ligands were both introduced initially (scenario 3) was also investigated. In scenario 2, mixing Cu^{2+} and ODA^{2-} resulted in a light blue suspension, which was changed to the typical slate-blue appearance upon the addition of the second ligand of AD^{-}. For other scenarios, similar slate-blue suspensions were resulted initially, insinuating the predominance of Cu^{2+}-AD^{-} interactions. (d-f) Temporal evolution of the sample PXRD patterns in scenarios (d) 1, (e) 2, and (f) 3, encompassing the initial mixing and subsequent heating stages. Despite different evolution pathways during room temperature mixing, the mixtures from all three scenarios generated pure BUT-321 crystals after 1 d heating, with the induction period < 1 h.

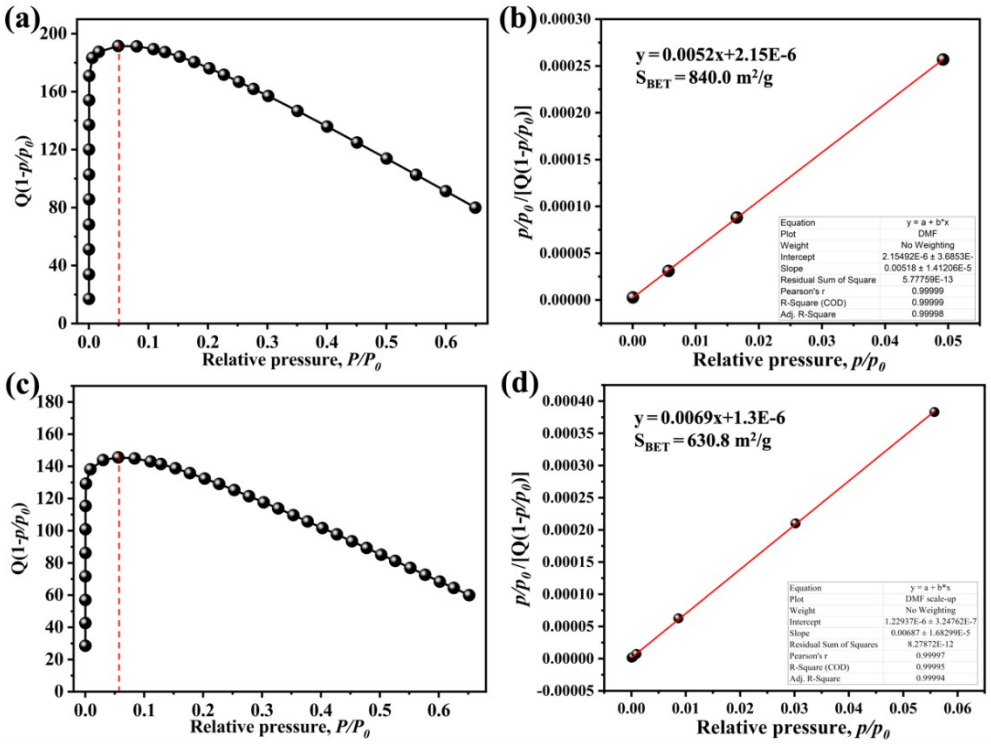

Figure S6. BET analysis of BUT-321 synthesized via traditional solvothermal method. Consistency plots and BET fitting plots of N_2 adsorption isotherms at 77 K are shown for (a, b) gram-scale sample and (c, d) large-scale sample (70 g).

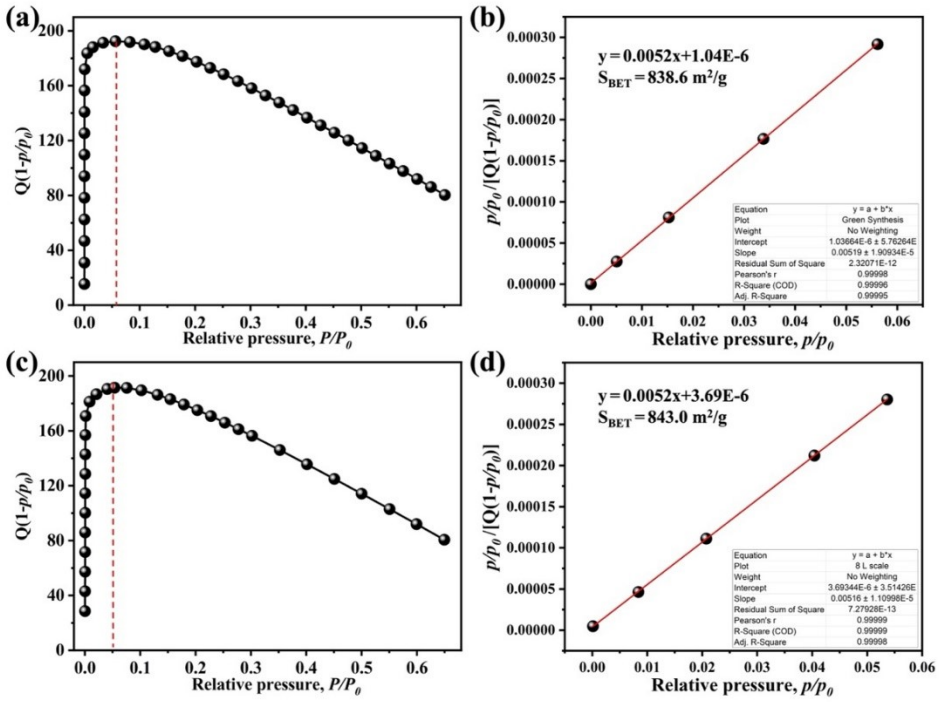

Figure S7. BET analysis of BUT-321 synthesized via green synthesis strategy. Consistency plots and BET fitting plots of N_2 adsorption isotherms at 77 K are shown for (a, b) gram-scale sample and (c, d) large-scale sample (kilogram scale).

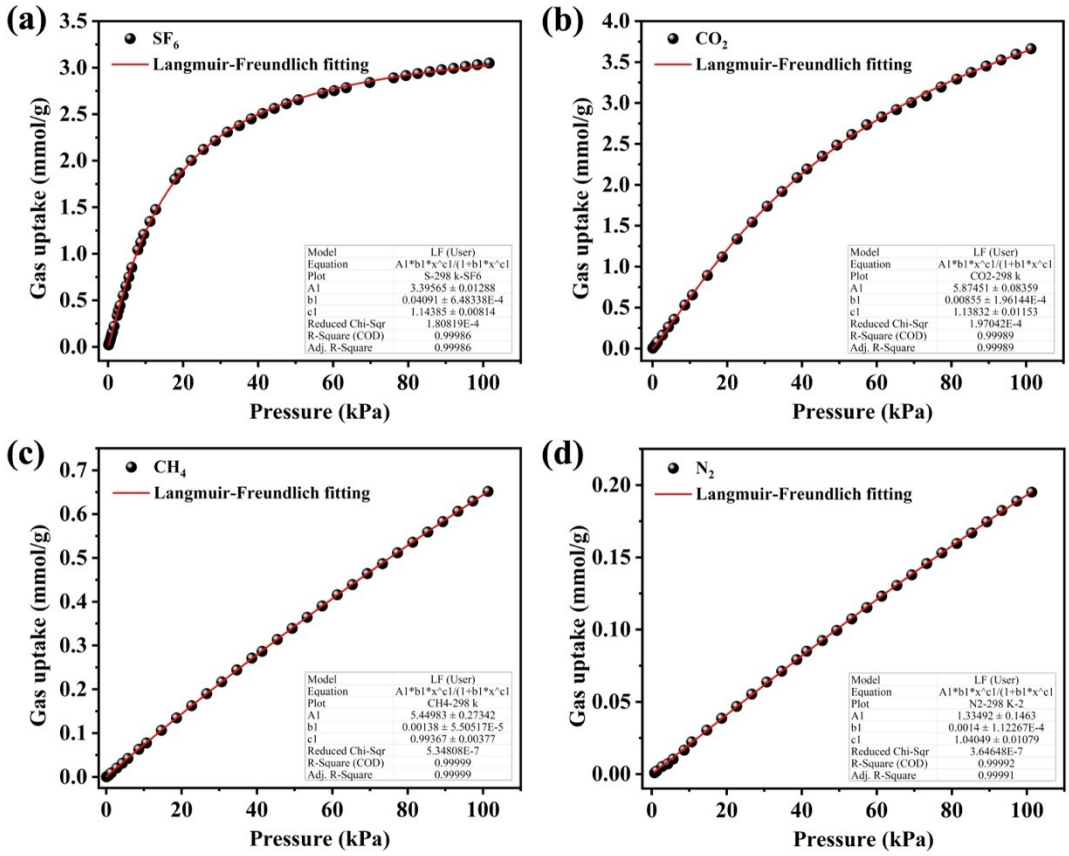

Figure S8. Langmuir-Freundlich fitting (red lines) of the adsorption isotherms (black points) of BUT-321-S. The adsorption isotherms at 298 K for (a) SF_6, (b) CO_2, (c) CH_4 and (d) N_2 are analyzed.

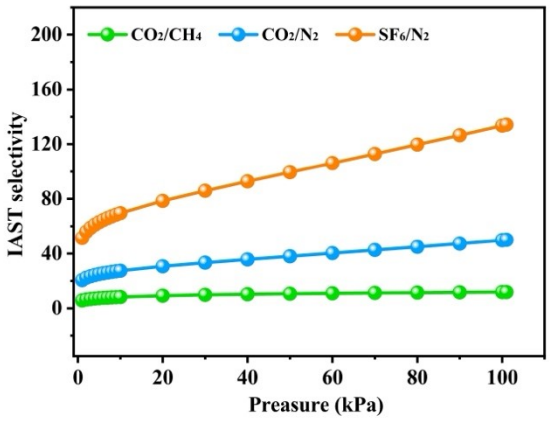

Figure S9. The IAST selectivity of BUT-321 calculated for SF_6/N_2 (orange), CO_2/N_2 (blue), and CO_2/CH_4 (green).

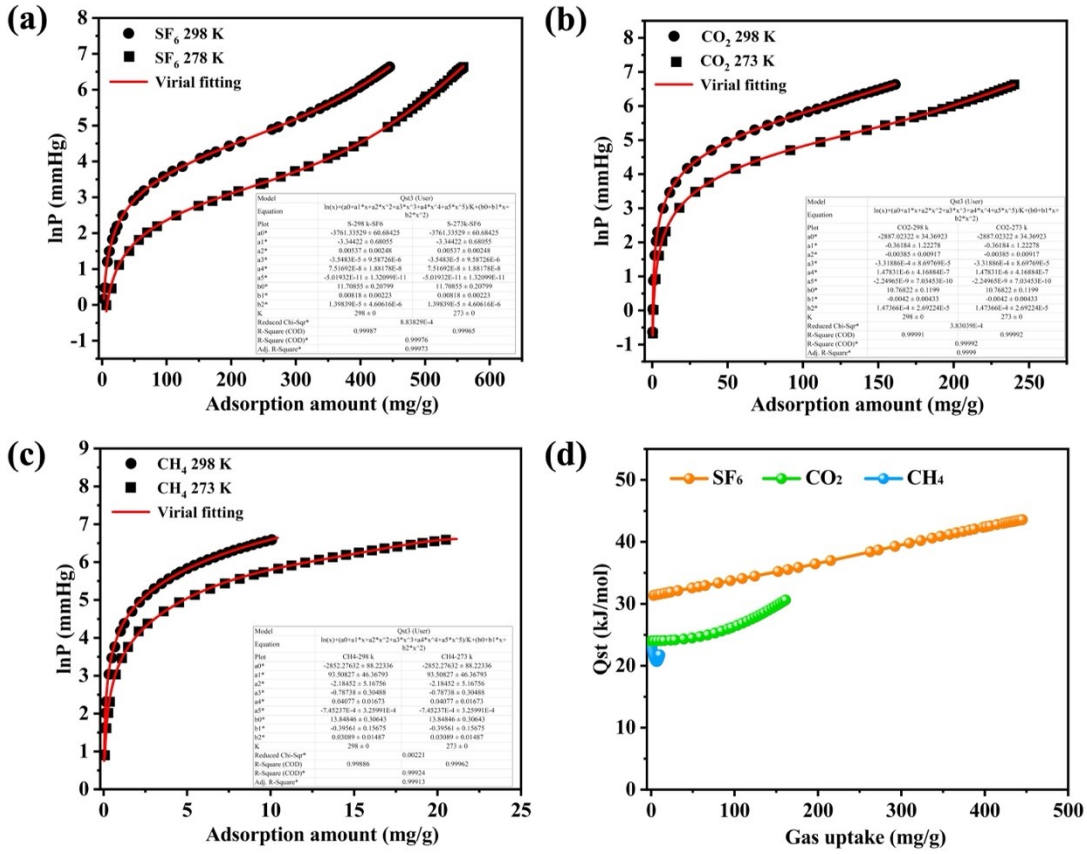

Figure S10. Virial fitting for Q_{st} calculation. The fitting of adsorption isotherms for (a) SF_6, (b) CO_2, and (c) CH_4 (black points) on BUT-321 at 273 and 298 K are demonstrated. (d) Coverage-dependent isosteric heats of SF_6 (orange), CO_2 (green), and CH_4 (blue) on BUT-321. The calculated Q_{st} at near-zero coverage is 31.4, 24.0 and 23.7 kJ mol^{-1} for SF_6, CO_2, and CH_4, respectively.

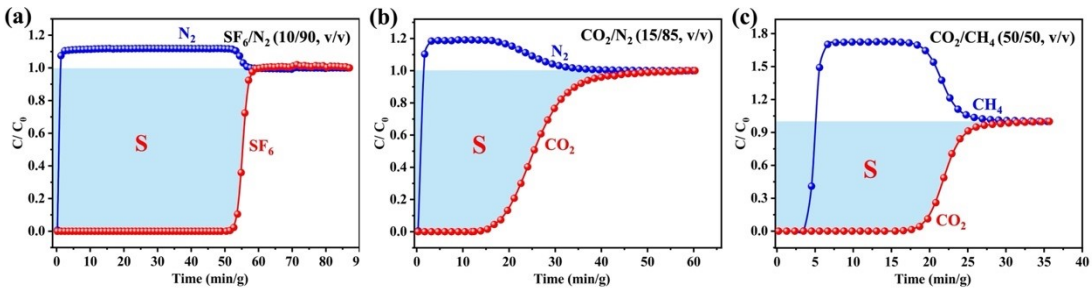

Figure S11. The calculation of dynamic SF_6 and CO_2 adsorption capacities on BUT-321-S. The corresponding adsorption capacities are estimated to be 27.4 cm^3/g, 19.5 cm^3/g and 54.9 cm^3/g for (a) SF_6/N_2 (10/90, v/v), (b) CO_2/N_2 (15/85, v/v) and (c) CO_2/CH_4 (50/50, v/v), based on the shaded areas in breakthrough curves.

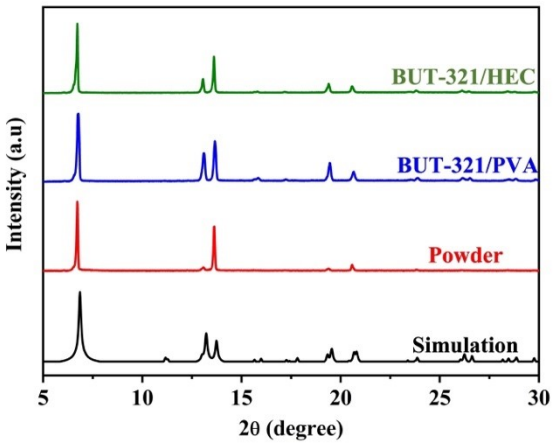

Figure S12. PXRD patterns of shaped BUT-321 pellets using PVA or HEC as the binder. Compared with BUT-321 powder, all the characteristic diffraction peaks were well preserved, demonstrating the structural integrity throughout the shaping process.

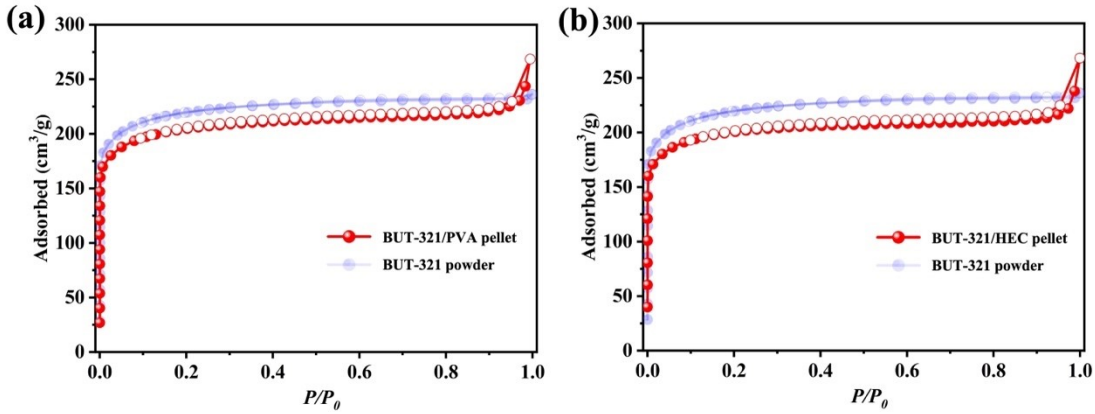

Figure S13. N_2 adsorption isotherms of BUT-321/HEC pellet (a) and BUT-321/PVA pellet (b). The isotherm of BUT-321 powder under the same condition is shown in semitransparent as a comparison. The negligible loss in N_2 uptakes at 77 K prove that both binders had little effect on the porosity of BUT-321.

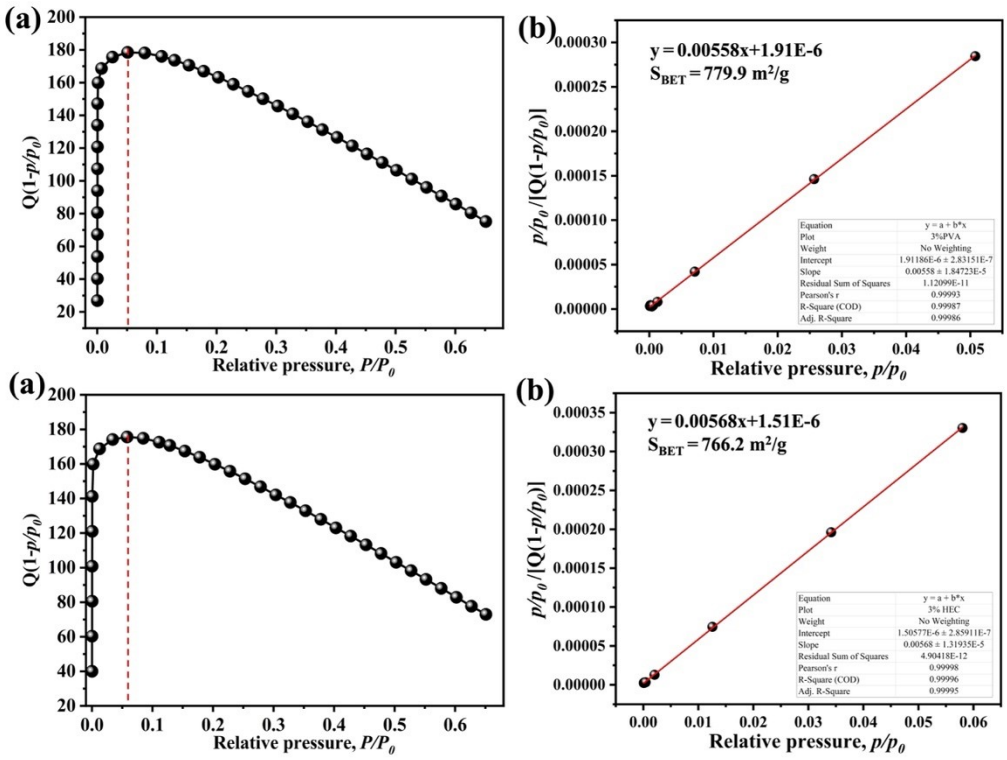

Figure S14. The consistency plots (a, c) and calculation plots of surface areas (b, d) for (a, b) BUT-321/PVA and (c, d) BUT-321/HEC pellets. The calculations are based on their N_2 adsorption isotherms at 77 K.

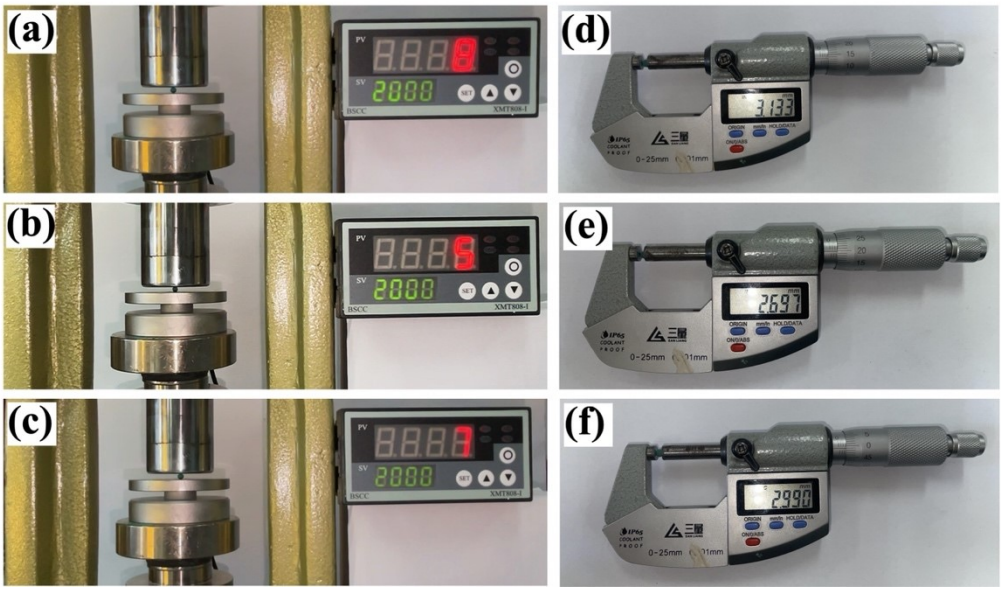

Figure S15. Mechanical strength measurements (a-c) and the corresponding diameters (d-f) of BUT-321 pellets prepared with the PVA binder. The average mechanical strength, determined by testing three randomly selected pellets, was 2.25 N/mm.

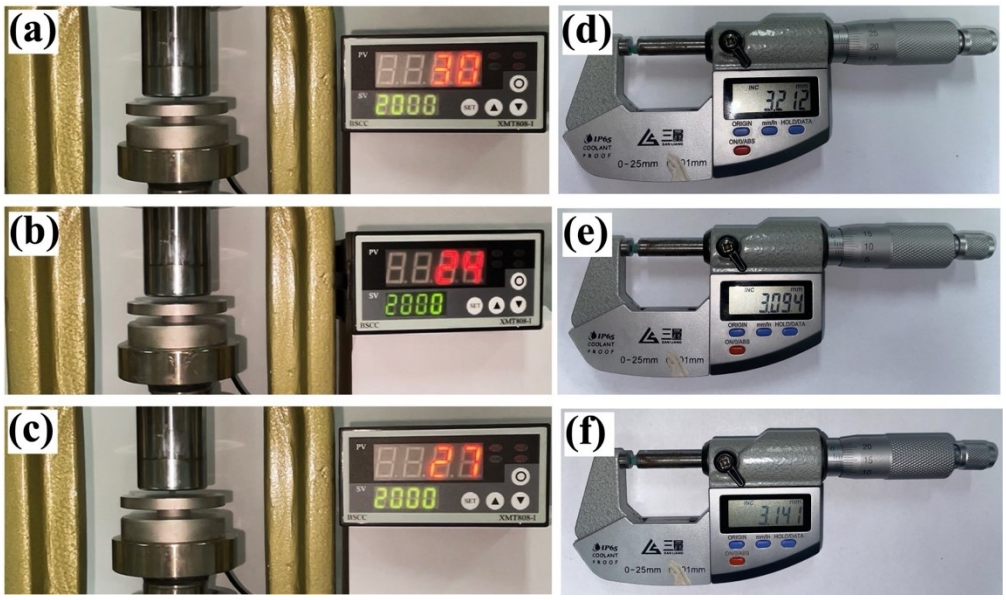

Figure S16. Mechanical strength measurements (a-c) and the corresponding diameters (d-f) of BUT-321 pellets prepared with the HEC binder. The average mechanical strength, determined by testing three randomly selected pellets, was 8.57 N/mm.

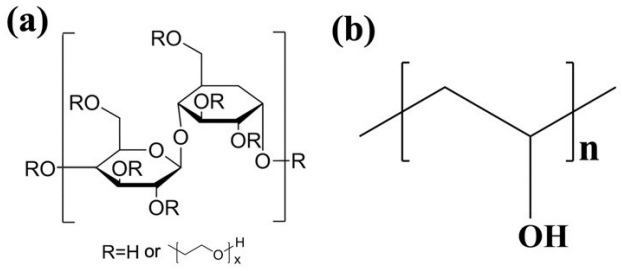

Figure S17. The chemical formulas of HEC (a) and PVA (b). Compared to their PVA counterparts, the higher mechanical strength of BUT-321/HEC pellets is attributed to a greater number of hydroxyl groups and the entanglement of the side chains of HEC molecules.

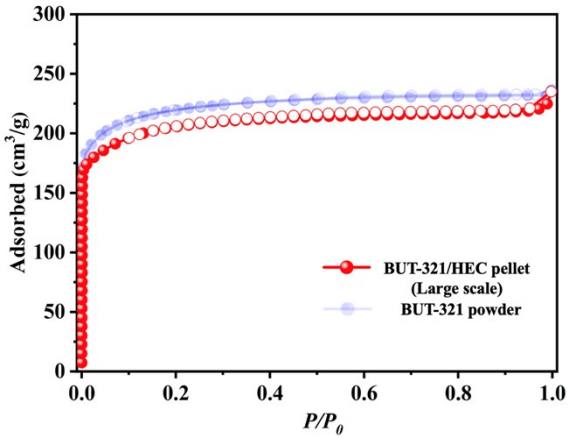

Figure S18. N_2 adsorption isotherm of BUT-321/HEC pellets fabricated on a large scale via a semi-automatic granulator. The isotherm of BUT-321 powder under the same condition is shown in semitransparent as a comparison. Negligible capacity loss indicates that scaling up the pelletization process exerts trivial influences on the adsorption performance of BUT-321 samples.

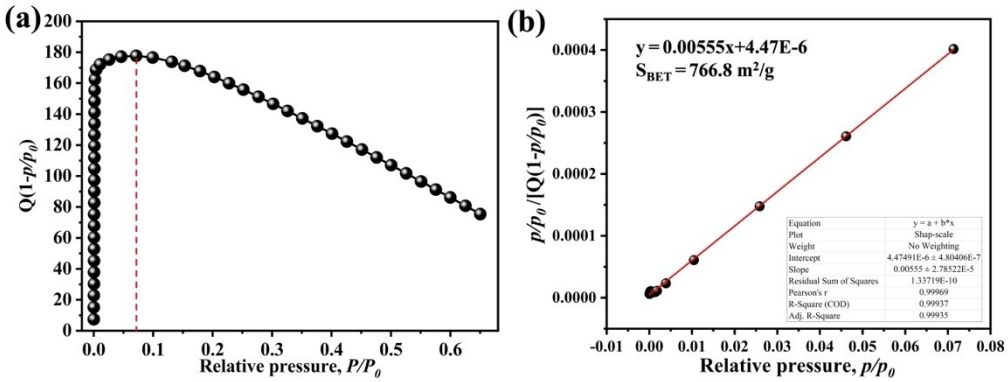

Figure S19. The consistency plot (a) and the BET surface area calculation (b) for the large-scale BUT-321/HEC pellets, derived from their N_2 adsorption isotherm measured at 77 K.

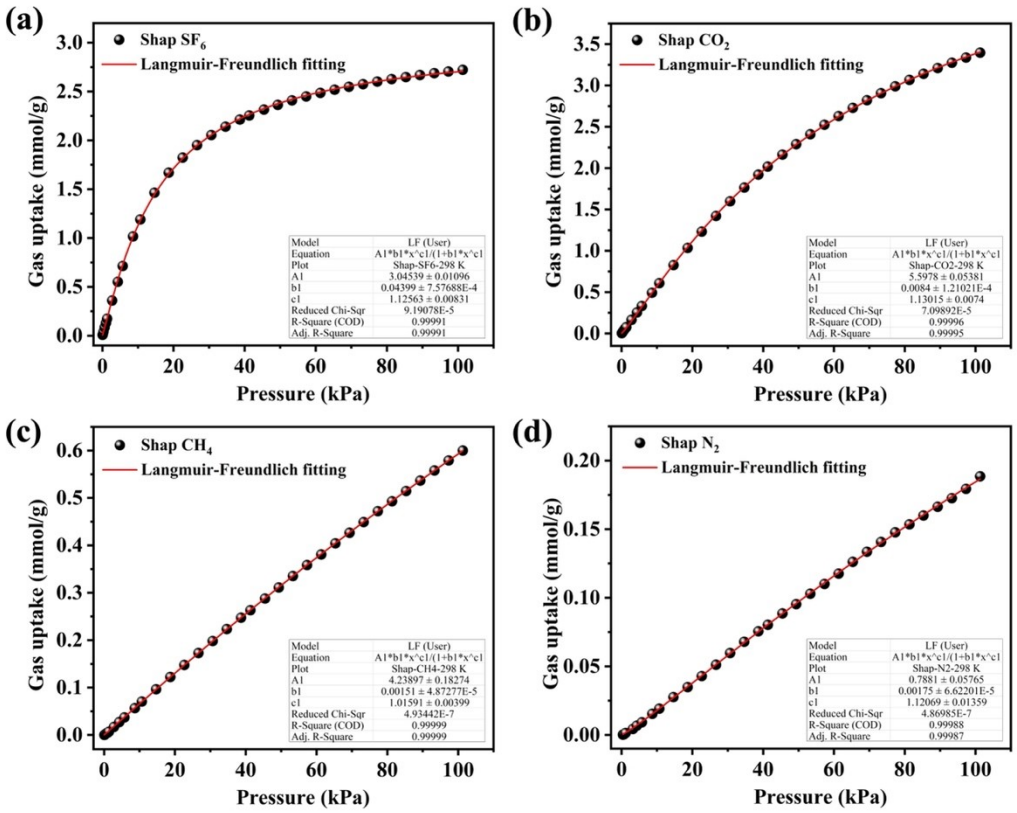

Figure S20. Langmuir-Freundlich fitting (red lines) of the adsorption isotherms (black points) of shaped BUT-321/HEC pellets. The adsorption isotherms at 298 K for (a) SF_6, (b) CO_2, (c) CH_4 and (d) N_2 are analyzed.

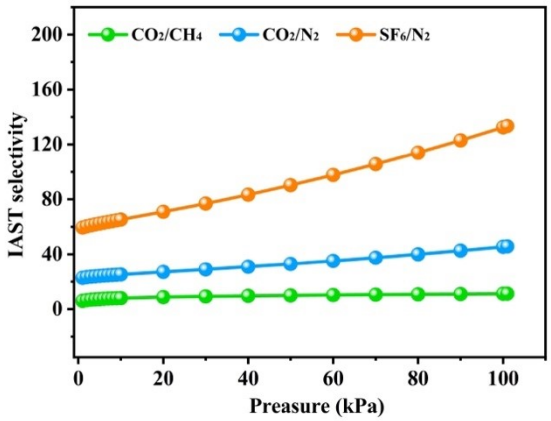

Figure S21. The IAST selectivity of shaped BUT-321 for SF_6/N_2 (orange), CO_2/N_2 (blue), and CO_2/CH_4 (green).

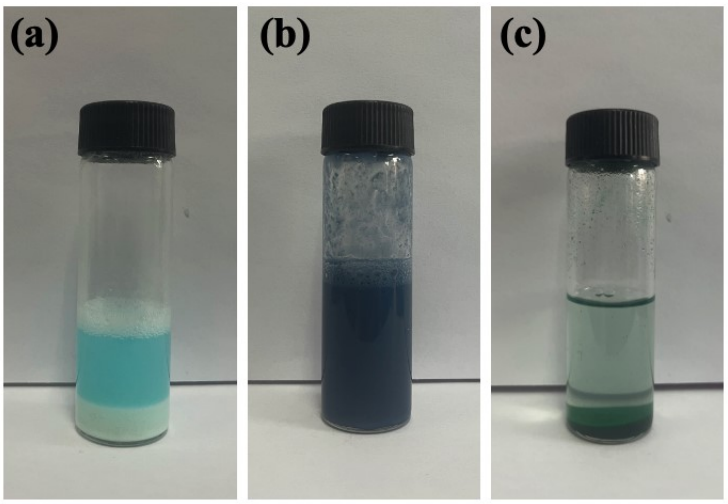

Figure S22. Visual demonstration of the reconstruction process of spent MOF pellets. (a) Degraded MOF pellets immersed in a H_2SO_4-acidified post-synthesis supernatant, forming a light blue solution and white precipitates. (b) Formation of the typical slate-blue appearance upon the addition of NaOH. (c) Successfully reborn BUT-321 crystals after heating, featuring the characteristic green color.

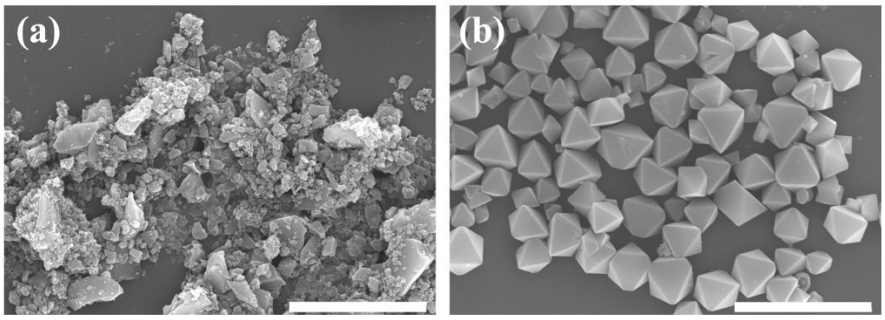

Figure S23. Electron micrographs of (a) damaged and (b) reborn BUT-321 samples before and after the acid-base recycling process. Scale bars equal 20 μm.

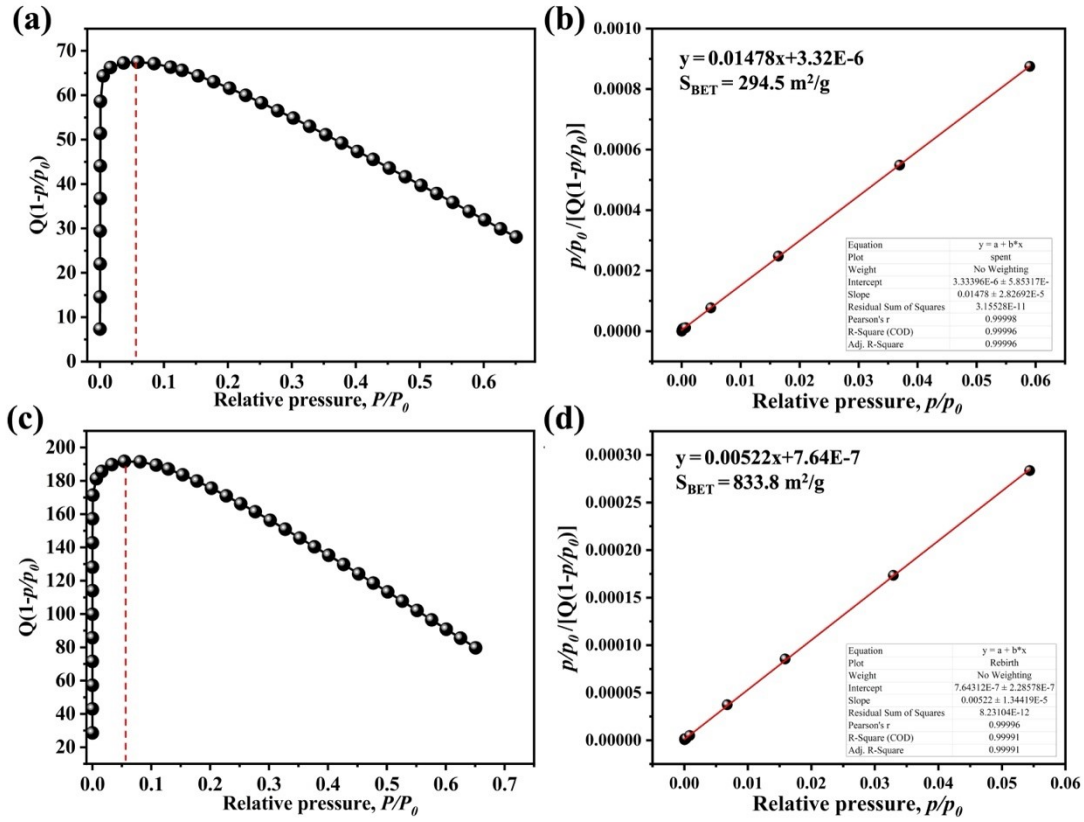

Figure S24. (a, c) Consistency plots and (b, d) surface area calculation plots for (a, b) spent BUT-321 pellets and (c, d) reborn BUT-321 crystals. The calculation is based on their N_2 adsorption isotherms at 77 K.

References

1 P.-D. Zhang, J.-H. Liu, X.-Q. Wu, Y. Xie, J. Yu and J.-R. Li, *Sep. Purif. Technol.*, 2024, **333**, 125791.

2 D. J. C. Constable, A. D. Curzons and V. L. Cunningham, *Green Chem.*, 2002, **4**, 521-527.

3 J. VandeVondele, M. Krack, F. Mohamed, M. Parrinello, T. Chassaing and J. Hutter, *Comput. Phys. Commun.*, 2005, **167**, 103-128.

4 M. Krack and M. Parrinello, *Phys. Chem. Chem. Phys.*, 2000, **2**, 2105-2112.

5 C. Hartwigsen, S. Goedecker and J. Hutter, *Phys. Rev. B*, 1998, **58**, 3641-3662.

6 S. Goedecker, M. Teter and J. Hutter, *Phys. Rev. B*, 1996, **54**, 1703-1710.

7 J. VandeVondele and J. Hutter, *J. Chem. Phys.*, 2007, **127**, 114105.

8 J. P. Perdew, K. Burke and M. Ernzerhof, *Phys. Rev. Lett.*, 1996, **77**, 3865.

9 S. Grimme, J. Antony, S. Ehrlich and H. Krieg, *J. Chem. Phys.*, 2010, **132**, 154104.

10 P.-D. Zhang, X.-Q. Wu, Q. Shuai, J. Yu, X. Zhang and J.-R. Li, *ACS Mater. Lett.*, 2024, **6**, 4632-4638.

11 S.-M. Li, Q. Zhang, H.-C. Jiang, Q.-L. Ni, L.-C. Gui, X.-J. Wang and T.-L. Hu, *Chem. Eng. J.*, 2024, **496**, 154026.

12 M.-B. Kim, K.-M. Kim, T.-H. Kim, T.-U. Yoon, E.-J. Kim, J.-H. Kim and Y.-S. Bae, *Chem. Eng. J.*, 2018, **339**, 223-229.
13 M. Åhlén, E. Kapaca, D. Hedbom, T. Willhammar, M. Strømme and O. Cheung, *Micropor. Mesopor. Mater.*, 2022, **329**, 111548.
14 M.-B. Kim, S.-J. Lee, C. Y. Lee and Y.-S. Bae, *Micropor. Mesopor. Mater.*, 2014, **190**, 356-361.
15 S.-M. Wang, X.-T. Mu, H.-R. Liu, S.-T. Zheng and Q.-Y. Yang, *Angew. Chem. Int. Ed.*, 2022, **61**, e202207066.
16 M. Åhlén, F. M. Amombo Noa, L. Öhrström, D. Hedbom, M. Strømme and O. Cheung, *Micropor. Mesopor. Mater.*, 2022, **343**, 112161.
17 C. Y. Chuah, K. Goh and T.-H. Bae, *J. Phys. Chem. C*, 2017, **121**, 6748-6755.
18 Y. Hu, L. Wang, R. Nan, N. Xu, Y. Jiang, D. Wang, T. Yan, D. Liu, Y. Zhang and B. Chen, *Chem. Eng. J.*, 2023, **471**, 144851.
19 T. Wang, M. Chang, T. Yan, Y. Ying, Q. Yang and D. Liu, *Ind. Eng. Chem. Res.*, 2021, **60**, 5976-5983.
20 Y. Wu, T. Yan, W. Zhang, S. Chen, Y. Fu, Z. Zhang and H. Ma, *Ind. Eng. Chem. Res.*, 2022, **61**, 13603-13611.
21 J.-W. Yan, S.-Q. Gang, Z.-Y. Liu, H.-Y. Xu, R. Wang and J.-L. Du, *Sep. Purif. Technol.*, 2023, **327**, 124929.
22 X. Zhang, Y.-L. Zhao, X.-Y. Li, X. Bai, Q. Chen and J.-R. Li, *J. Am. Chem. Soc.*, 2024, **146**, 19303-19309.
23 S.-T. Zheng, R.-Y. Jiang, Y. Jiang, S. Ni, G.-W. Guan, S.-Q. Shao, Y.-C. Wang, S.-M. Wang and Q.-Y. Yang, *Sep. Purif. Technol.*, 2023, **318**, 123957.
24 H.-R. Liu, S.-M. Wang, Y.-L. Dong, S.-T. Zheng, S. Ni, J. Xu and Q.-Y. Yang, *Chinese J. Struc. Chem.*, 2023, **42**, 100022.
25 J. Ren, M. Chang, W. Zeng, Y. Xia, D. Liu, G. Maurin and Q. Yang, *Chem. Mater.*, 2021, **33**, 5108-5114.
26 M. Chang, T. Yan, Y. Wei, J.-X. Wang, D. Liu and J.-F. Chen, *Chem. Mater.*, 2022, **34**, 9134-9143.
27 L. Yan, H.-T. Zheng, L. Song, Z.-W. Wei, J.-J. Jiang and C.-Y. Su, *Chem. Eng. J.*, 2023, **472**, 145145.
28 M. Yang, M. Chang, T. Yan and D. Liu, *Sep. Purif. Technol.*, 2022, **295**, 121340.
29 M. Åhlén, Y. Zhou, D. Hedbom, H. S. Cho, M. Strømme, O. Terasaki and O. Cheung, *J. Mater. Chem. A*, 2023, **11**, 26435-26441.
30 Q. Fan, J. Yao, S. Zhao, X. Wu, J. Huang, H. Luo and Q. Xia, *Small*, 2025, **21**, 2409215.
31 P.-J. Kim, Y.-W. You, H. Park, J.-S. Chang, Y.-S. Bae, C.-H. Lee and J.-K. Suh, *Chem. Eng. J.*, 2015, **262**, 683-690.
32 Y. Cao, Y. Zhao, Z. Lv, F. Song and Q. Zhong, *J. Ind. Eng. Chem.*, 2015, **27**, 102-107.
33 S. R. Caskey, A. G. Wong-Foy and A. J. Matzger, *J. Am. Chem. Soc.*, 2008, **130**, 10870-10871.
34 S.-M. Wang, H.-R. Liu, S. Ni and Q.-Y. Yang, *Chinese J. Chem.*, 2023, **41**, 763-768.

35 M. Sakai, A. Ito, T. Matsumoto and M. Matsukata, *Chem. Lett.*, 2024, **53**.
36 J.-B. Lin, T. T. T. Nguyen, R. Vaidhyanathan, J. Burner, J. M. Taylor, H. Durekova, F. Akhtar, R. K. Mah, O. Ghaffari-Nik, S. Marx, N. Fylstra, S. S. Iremonger, K. W. Dawson, P. Sarkar, P. Hovington, A. Rajendran, T. K. Woo and G. K. H. Shimizu, *Science*, 2021, **374**, 1464-1469.
37 B. Chen, D. Fan, R. V. Pinto, I. Dovgaliuk, S. Nandi, D. Chakraborty, N. García-Moncada, A. Vimont, C. J. McMonagle, M. Bordonhos, A. Al Mohtar, I. Cornu, P. Florian, N. Heymans, M. Daturi, G. De Weireld, M. Pinto, F. Nouar, G. Maurin, G. Mouchaham and C. Serre, *Adv. Sci.*, 2024, **11**, 2401070.
38 D. Lv, J. Chen, K. Yang, H. Wu, Y. Chen, C. Duan, Y. Wu, J. Xiao, H. Xi, Z. Li and Q. Xia, *Chem. Eng. J.*, 2019, **375**, 122074.
39 P. Nugent, Y. Belmabkhout, S. D. Burd, A. J. Cairns, R. Luebke, K. Forrest, T. Pham, S. Ma, B. Space, L. Wojtas, M. Eddaoudi and M. J. Zaworotko, *Nature*, 2013, **495**, 80-84.
40 H. Lyu, O. I.-F. Chen, N. Hanikel, M. I. Hossain, R. W. Flaig, X. Pei, A. Amin, M. D. Doherty, R. K. Impastato, T. G. Glover, D. R. Moore and O. M. Yaghi, *J. Am. Chem. Soc.*, 2022, **144**, 2387-2396.
41 H.-M. Wen, C. Liao, L. Li, A. Alsalme, Z. Alothman, R. Krishna, H. Wu, W. Zhou, J. Hu and B. Chen, *J. Mater. Chem. A*, 2019, **7**, 3128-3134.
42 L. Yang, X. Cui, Y. Zhang, Q. Wang, Z. Zhang, X. Suo and H. Xing, *Acs Sustain. Chem. Eng.*, 2019, **7**, 3138-3144.
43 F. Shen, J. Wu, G. Chen, Z. Wei, J. Wang, Z. Lin and K. Chai, *J. Environ. Chem. Eng.*, 2024, **12**, 113796.
44 H. A. Evans, D. Mullangi, Z. Deng, Y. Wang, S. B. Peh, F. Wei, J. Wang, C. M. Brown, D. Zhao, P. Canepa and A. K. Cheetham, *Sci. Adv.*, **8**, eade1473.
45 D. Song, F. Jiang, D. Yuan, Q. Chen and M. Hong, *Small*, 2023, **19**, 2302677.
46 L. Du, Y. Miao, B. Zheng, M. Ma and J. Zhang, *J. Solid. State Chem.*, 2021, **300**, 122230.
47 H. Wu, Y. Yuan, Y. Chen, D. Lv, S. Tu, Y. Wu, Z. Li and Q. Xia, *Energ. Fuel.*, 2021, **35**, 610-617.
48 Q. Liu, S. G. Cho, J. Hilliard, T.-Y. Wang, S.-C. Chien, L.-C. Lin, A. C. Co and C. R. Wade, *Angew. Chem. Int. Ed.*, 2023, **62**, e202218854.
49 L. Hu, W. Wu, L. Jiang, M. Hu, H. Zhu, L. Gong, J. Yang, D. Lin and K. Yang, *Acs Appl. Mater. Inter.*, 2023, **15**, 43925-43932.
50 B. Shan, J. Yu, M. R. Armstrong, D. Wang, B. Mu, Z. Cheng and J. Liu, *AIChE J.*, 2017, **63**, 4532-4540.
51 J. McEwen, J.-D. Hayman and A. Ozgur Yazaydin, *Chem. Phys.*, 2013, **412**, 72-76.
52 Y. Chen, Z. Qiao, J. Huang, H. Wu, J. Xiao, Q. Xia, H. Xi, J. Hu, J. Zhou and Z. Li, *ACS Appl. Mater. Inter.*, 2018, **10**, 38638-38647.
53 P. Singh, H. D. Singh, A. H. Menon and R. Vaidhyanathan, *Chem. Commun.*, 2023, **59**, 5559-5562.
54 Z. Shi, Y. Tao, J. Wu, C. Zhang, H. He, L. Long, Y. Lee, T. Li and Y.-B. Zhang, *J. Am. Chem. Soc.*, 2020, **142**, 2750-2754.

55 X. Chen, D. Menon, X. Wang, M. He, M. R. A. Kiapi, M. Asgari, Y. Lyu, X. Tang, L. L. Keenan, W. Shepard, L. H. Wee, S. Yang, O. K. Farha and D. Fairen-Jimenez, *Chem*, 2025, **11**, 102382.
56 Y. Chen, K. Wang, J.-H. Li, Y. Wang, R.-B. Lin, X.-M. Chen, J. Li and L. Li, *Adv. Mater.*, 2025, **37**, 2410500.
57 M. Jiang, J. Hu, Y. Zhang, Y. Chen, L. Jin, Y. Chen, Y. Lai, R. Krishna, P. Hu and H. Ji, *ACS Mater. Lett.*, 2025, **7**, 1242-1249.
58 J. Peng, C. Fu, J. Zhong, B. Ye, J. Xiao, C. Duan and D. Lv, *Journal*, 2023, **28**.
59 J. Dai, D. Xie, Y. Liu, Z. Zhang, Y. Yang, Q. Yang, Q. Ren and Z. Bao, *Ind. Eng. Chem. Res.*, 2020, **59**, 7866-7874.